J Therm Anal Calorim (2012) 110:799–805
DOI 10.1007/s10973-011-2016-5

An investigation of decomposition stages of a ruthenium polypridyl complex by non-isothermal methods

Fatih M. Emen · Kasim Ocakoglu · Nevzat Kulcu

Received: 20 July 2011 / Accepted: 19 October 2011 / Published online: 2 November 2011

Abstract Thermal properties of [*cis*-(dithiocyanato)(4,5-diazafluoren-9-one)(4,4′-dicarboxy-2,2′-bipyridyl)ruthenium (II)], $[Ru(L_1)(L_2)(NCS)_2]$ (where the ligands L_1 =4,5-diazafluoren-9-one, L_2 = 4,4′-dicarboxy-2,2′-bipyridyl) have been investigated by DTA/TG/DTG measurements under inert atmosphere in the temperature range of 30–1155 °C. The mass spectroscopy technique has been used to identify the products during pyrolytic decomposition. The pyrolytic final products have been analyzed by X-ray powder diffraction technique. A decomposition mechanism has been also suggested for the *cis*-$[Ru(L_1)(L_2)(NCS)_2]$ complex based on the results of thermogravimetrical and mass analysis. The values of the activation energy, E^* have been obtained by using model-free Kissenger–Akahira–Sunose and Flyn–Wall–Ozawa non-isothermal methods for all decomposition stages. Thirteen kinetic model equations have been tested for selecting the best reaction models. The best model equations have been determined as A2, A3, D1, and D2 which correspond to nucleation and growth mechanism for A2 and A3 and diffusion mechanism for D1 and D2. The optimized average values of E^* are 31.35, 58.48, 120.85, and 120.56 kJ mol^{-1} calculated by using the best model equations for four decomposition stages, respectively. Also, the average Arrhenius factor, A, has been obtained as 2.21, 2.61, 2.52, and 2.21 kJ mol^{-1} using the best model equation for four decomposition stages, respectively. The ΔH^*, ΔS^*, and ΔG^* functions have been calculated using the optimized values.

Keywords Ruthenium complex · Thermal behavior · Dye sensitized solar cell · Polypyridyl complexes · Photosensitizer · Charge transfer sensitizer

F. M. Emen (✉)
Department of Chemistry, Faculty of Arts and Science, Kirklareli University, 39300 Kirklareli, Turkey
e-mail: femen106@gmail.com

K. Ocakoglu (✉)
Advanced Technology Research & Application Center, Mersin University, Yenisehir, 33343 Mersin, Turkey
e-mail: kasim.ocakoglu@mersin.edu.tr

N. Kulcu
Department of Chemistry, Faculty of Arts and Science, Mersin University, 33343 Mersin, Turkey

Introduction

Ruthenium-(II) bipyridine-type complexes with polypyridyl ligands are very useful building blocks for the construction of supramolecular species capable of exhibiting peculiar photochemical stability, strong visible absorption, efficient luminescence, and a relatively long lived metal to ligand charge transition (MLCT) [1–10]. Ruthenium-(II) bipyridine complexes have been the focus of considerable attention for the past half century because of the best photovoltaic performance in photovoltaic applications in terms of both conversion yield and long-term stability. Recently, these studies have received further interest because of their potential application of polypyridyl compounds in the development of sustainable and environmentally friendly energy [11–13]. Several ruthenium complexes have been used as dyes for photovoltaic applications [1–8]. In these complexes, the anchoring groups such as carboxylic acid, dihydroxy, and phosphonic acid on pyridine ligands serve to immobilize the dye on the nanocrystalline TiO_2 surface. Structural properties and applications of ruthenium-(II) polypyridine complexes have been studied extensively but thermal properties of these compounds are rarely investigated in the literature [14]. Thermal properties of these

complexes have critical importance especially for solar cell applications because of the requirement of long-term stability of the sensitizer under the operating conditions.

The [*cis*-(dithiocyanato)(4,5-diazafluoren-9-one)(4,4′-dicarboxy-2,2′-bipyridyl)ruthenium(II)], [Ru(L_1)(L_2)(NCS)$_2$] (where the ligands L_1 = 4,5-diazafluoren-9-one, L_2 = 4,4′-dicarboxy-2,2′-bipyridyl) were synthesized and characterized in our previous study [3]. In the present study, we have studied the thermal behavior of the [Ru(L_1)(L_2)(NCS)$_2$] complex. Based on the results of thermogravimetrical and mass analysis the decomposition mechanism for the [Ru(L_1)(L_2)(NCS)$_2$] complex has been suggested. The values of the activation energy, E^* have been calculated by model-free Kissenger–Akahira–Sunose (KAS) and Flyn–Wall–Ozawa (FWO) methods [15–32]. The 13 model equations have been tested for the best kinetic models giving the highest linear regression, the lowest standard deviation and giving the E^* values in good agreement with those calculated from model-free KAS and FWO methods. The optimized value of the E^* and A have been calculated using the best equation. Also, the other thermodynamic functions (ΔH^*, ΔS^* and ΔG^*) have been obtained using these values.

Experimental

All organic solvents were supplied by Fluka, and used as received. [RuCl$_2$(*p*-cymene)]$_2$, 4,5-diazafluoren-9-one (L_1), and 2,2′-bipyridine-4,4′-dicarboxylic acid (L_2) were purchased from Aldrich. The [Ru(L_1)(L_2)(NCS)$_2$] complex (Fig. 1) was synthesized according to the literature [3]. The DTA/TG/DTG curves were obtained by a Shimadzu DTG-60H equipped with DTA and TG units. Measurements of thermal analysis were performed in the range of 30–1155 °C using α-Al$_2$O$_3$ as a reference material while samples were in Pt crucibles. Measurements were performed in a dynamic nitrogen furnace atmosphere with a flow rate of 50 mL/min. Different heating rates were used such as 5, 10, and 15 °C/min and the mass samples were ranged from 6 to 10 mg. LG/MS–ESI measurement was carried out by an AGILENT 1100 MSD instrument to identify the gas decomposition products. X-ray powder diffraction (XRD) analysis of the final residue was made with a Siemens F model diffractometer equipped with an X-ray generator, Phillips, PW-1010 model ranging from 20 to 40 kV and 6–50 mA using a finely focused CuK$_\alpha$ radiation (λ = 1.5406 Å).

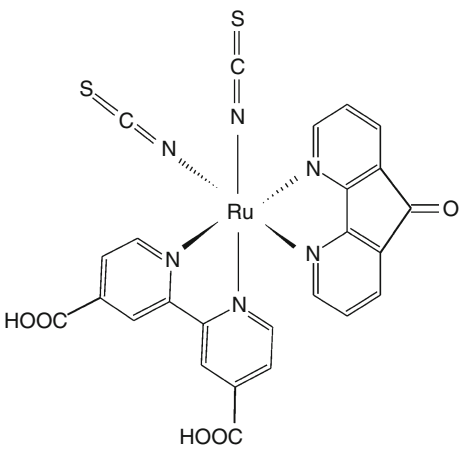

Fig. 1 The chemical structure of the *cis*-[Ru(L_1)(L_2)(NCS)$_2$] complex

Results and discussion

The thermal stability of the *cis*-[Ru(L_1)(L_2)(NCS)$_2$] complex

The decomposition temperature range, DTA minima peak positions, percentage of mass losses, and evolved moieties of the decomposition reactions are summarized in Table 1.

Thermal decomposition of the *cis*-[Ru(L_1)(L_2)(NCS)$_2$] complex

The DTA/TG/DTG curves of the ruthenium complex obtained in the temperature range of 25–1155 °C are shown in Fig. 2. It can be observed from the TG and DTG curves that the *cis*-[Ru(L_1)(L_2)(NCS)$_2$] complex exhibits four different decomposition stages. In the first stage, 1 mol H_2O left out in the temperature range of 30–117 °C with a mass loss 2.66% (calc. 2.58%). This result is also compatible with IR measurement that exhibits a broad characteristic peak corresponding to OH group with hydrogen bonding at 3402 cm^{-1} [3]. The second decomposition stage at which 2 mol CO_2 and 1 mol CO left out of the intermediate products were observed in the temperature between 117 and 307 °C. The mass loss in these products was about 16.68% (calc. 16.63%). The intermediate product in the second stage was Ru(SCN)$_2$($C_{10}H_8N_2$)$_2$. In the third stage, the mass loss of 22.39% (calc. 22.36%) is observed in between 307 and 571 °C. In this stage, the groups that left out the Ru(SCN)$_2$($C_{10}H_8N_2$)$_2$ are 2C_5H_4N. The intermediate product of this step was determined to be [Ru(SCN)$_2$(C_5H_4N)$_2$]. At the final decomposition step in the 571–1155 °C range, the experimental mass loss of 34.66% (calc. 34.40%) corresponds to the departure of 2C_5H_4N, 2SCN and 2CN groups were observed. The final products to be Ru (JPDS File No: 88-1734) and (RuS_2 (JPDS File No: 80-0669) with black-gray color with the mass of 23.66% (calc. 24.03%) was identified by XRD technique. In the DTA curve of the ruthenium complex, three endothermic peaks were observed as seen in Fig. 2. The minima of the DTA curve are obtained

Table 1 Thermoanalytical results of the decomposition reactions of the *cis*-[Ru(L_1)(L_2)(NCS)$_2$] complex

Stage	$DTA_{min.}$/°C	TG temp. range/°C	Mass loss/%		Evolved moiety
			Exper.	Theor.	
I	58	30–117	2.66	2.58	$-H_2O$[a]
II	217	117–307	16.68	16.63	$-CO$, $-2CO_2$
III	–	307–571	22.39	22.36	$-2C_5H_4N$
IV	656	571–1155	34.61	34.40	$-2C_5H_4N$, $-2CN$, 2SCN
Residue	–	–	23.66	24.03	Ru + RuS_2

[a] In the course of thermogravimetric measurements, moisture content can be easily seen because of the hygroscopic properties of the complex

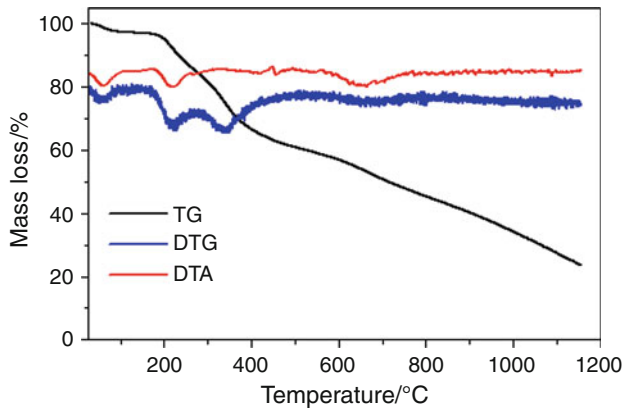

Fig. 2 TG/DTA/DTG curves of *cis*-[Ru(L_1)(L_2)(NCS)$_2$] complex

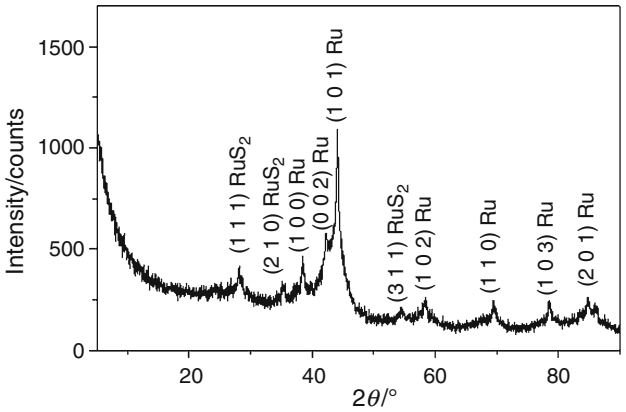

Fig. 3 XRD pattern of Ru (JCPDS File No: 88-1734) and RuS_2 (JCPDS File No: 80-0669) after the decomposition of the *cis*-[Ru(L_1)(L_2)(NCS)$_2$] complex

at 58, 217, and 656 °C, respectively. The first minimum corresponds to the elimination of H_2O and the other endothermic minima correspond to the decomposition of the *cis*-[Ru(L_1)(L_2)(NCS)$_2$] complex. The minima of the DTG curve observed at 58, 218, 340, and 653 °C demonstrate the four decomposition steps and the maximum speed of the mass loss.

According to the data of the TG, mass, and XRD measurements, the decomposition mechanism of the *cis*-[Ru(L_1)(L_2)(NCS)$_2$] complex can be given as in the Scheme 1. The XRD pattern and mass spectra can be seen in Figs. 3 and 4, respectively.

Decomposition kinetics of the *cis*-[Ru(L_1)(L_2)(NCS)$_2$] complex

As it is well known, the non-isothermal kinetic equations are used to determine the apparent kinetic parameters of the thermal decomposition reactions. According to results of International Congress on Thermal Analysis and Calorimetry (ICTAC) kinetic project, Isoconversional methods can be used extensively [33]. In Non-isothermal kinetics, KAS [19–21] and FWO [17, 18] methods are the most popular representatives of the isoconversional methods. In our kinetic study for the *cis*-[Ru(L_1)(L_2)(NCS)$_2$] complex, the KAS and FWO equations were used to determine the activation energy, E^* of the decomposition reactions for the conversion degree, α varying in the range of 0.05–0.95 in a step of 0.05. The ICTAC Kinetic Committee has recommended to determine the E^* values in a wide range of α between 0.05 and 0.95 with increments of 0.05 [34].

The kinetic equations are described as following:

KAS equation;

Scheme 1 The mechanism for the decomposition reaction of the *cis*-[Ru(L_1)(L_2)(NCS)$_2$] complex

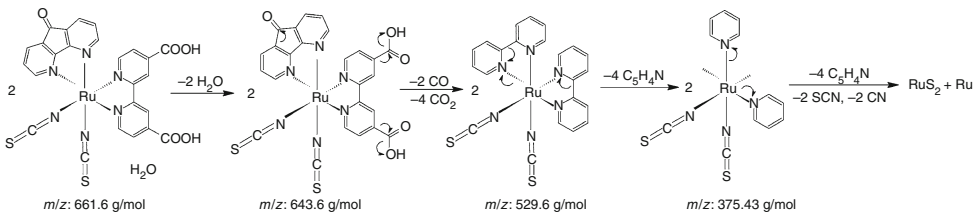

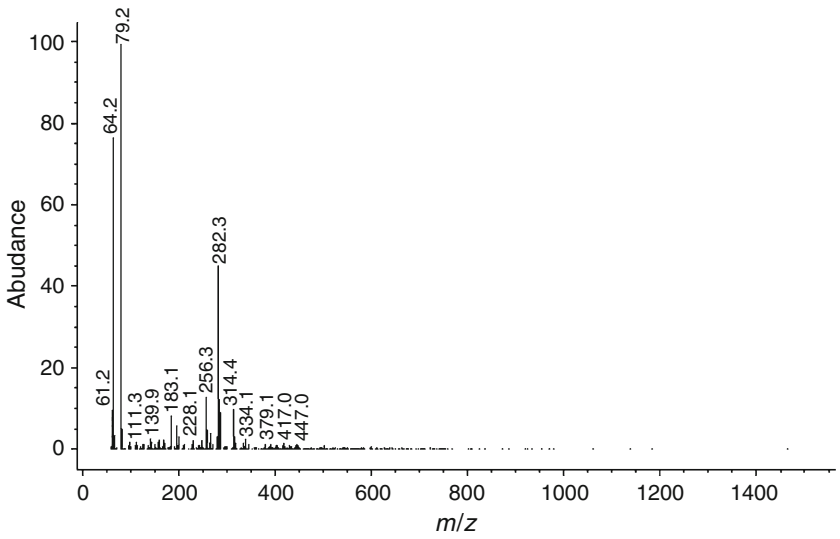

Fig. 4 Mass spectra of the *cis*-[Ru(L_1)(L_2)(NCS)$_2$] complex

$$\ln\frac{\beta}{T^2} = \ln\frac{AR}{g(\alpha)E*} - \frac{E*}{RT} \quad (1)$$

FWO equation;

$$\ln\beta = \left(\frac{AE*}{Rg(\alpha)}\right) - 5.3305 - 1.05178\frac{E*}{RT} \quad (2)$$

where β is the heating rate (K min^{-1}), A is pre-exponential factor (min^{-1}), R is the gas constant (8.314 J mol^{-1} K^{-1}), and T is the absolute temperature, K.

According to the aforementioned equations, the plots of $\ln\beta/T^2$ versus $1/T$ and $\ln\beta$ versus $1/T$ give parallel lines for each conversion, α value. The activation energies can be calculated from the slopes of each line with linear correlation coefficient, r. The activation energies, E^* of the decomposition process calculated by model-free KAS and FWO methods are given Table 2.

KAS and FWO equations have been re-arranged to find the kinetic triplet, E^*, A, $g(a)$ [34–38]. These methods are known as "composite method I" and "composite method II" in literature [35, 36].

Modeling KAS equation (composite method I, C.M I);

$$\ln\frac{g(\alpha)}{T^2} = \ln\frac{AR}{\beta E*} - \frac{E*}{RT} \quad (3)$$

Modeling FWO equation (composite method II, C.M II);

$$\ln g(\alpha) = \left(\frac{AE*}{\beta R}\right) - 5.3305 - 1.05178\frac{E*}{RT} \quad (4)$$

The plots of $\ln[g(\alpha)/T^2]$ versus 1/T (in composite method I), $\ln g(\alpha)$ versus $1/T$ (in composite method II) give parallel lines for each α value at single β value. The E^* and A values have been calculated for each model functions, $g(\alpha)$. The best kinetic model function giving activation energies in good agreement with those obtained using model-free KAS and FWO methods and also has the highest regression analysis and the lowest standard deviation. The changes of the entropy, ΔS^*, enthalpy, ΔH^* and Gibbs free energy, ΔG^* for the activated complex can be calculated using the thermodynamic equations;

Table 2 The values of the activation energy, E^* of the decomposition processes

Compound	Stage	FWO method E^*/kJ mol^{-1}	KAS method E^*/kJ mol^{-1}
Ruthenium complex[a]	I	19.82	20.14
	II	48.38	49.82
	III	108.82	113.23
	IV	112.09	117.01

[a] *Cis*-[Ru(L_1)(L_2)(NCS)$_2$] complex

$$A = (kT_{\text{avg.}}/h)e^{\Delta S*/R} \quad (5)$$

$$\Delta H* = E* - RT_{\text{avg.}} \quad (6)$$

$$\Delta G* = \Delta H* - T_{\text{avg.}}\Delta S* \quad (7)$$

where, E^* is the activation energy which is calculated from slope of modeling method curves for the most suitable model, k is the Boltzmann constant, h is the planck's constant, and T_{avg}. is average reaction temperature.

The dependencies of E^* versus α is very important for detecting the multi-step kinetics. If the value of E^* varies as α significantly, the decomposition process is kinetically complex [34, 37, 38].

The α which dependents on E^* of the *cis*-[Ru(L_1)(L_2)(NCS)$_2$] complex was calculated using each of the two methods. Each method shows similar tendency in each stage. The E^* versus α for the *cis*-[Ru(L_1)(L_2)(NCS)$_2$] complex based on model-free KAS and FWO methods are

shown for all decomposition stages in Fig. 5a–d, respectively.

In stage I, the E^* values calculated by KAS and FWO methods are quite similar. The E^* values increase up to $\alpha = 0.15$ and then decrease up to $\alpha = 0.4$. The E^* values slightly change in the conversion degree range of 0.4–0.9. Finally, the E^* values increase in the range of $0.9 \leq \alpha \leq 0.95$ (Fig. 5a). Therefore, it is concluded that the decompositions contain multi-step kinetics. The reversible dehydration process tend to give a decreasing E^* versus α dependence [33]. The average E^* values are 20.14, 19.82 kJ mol^{-1} calculated by KAS and FWO methods, respectively.

In stage II, the E^* values calculated by using KAS and FWO methods are quite similar too. The E^* values increase as α increase up to 0.7 and then start to decrease (Fig. 5b). Therefore, it is concluded that the decomposition takes place at least in two steps. The complex compounds tend to

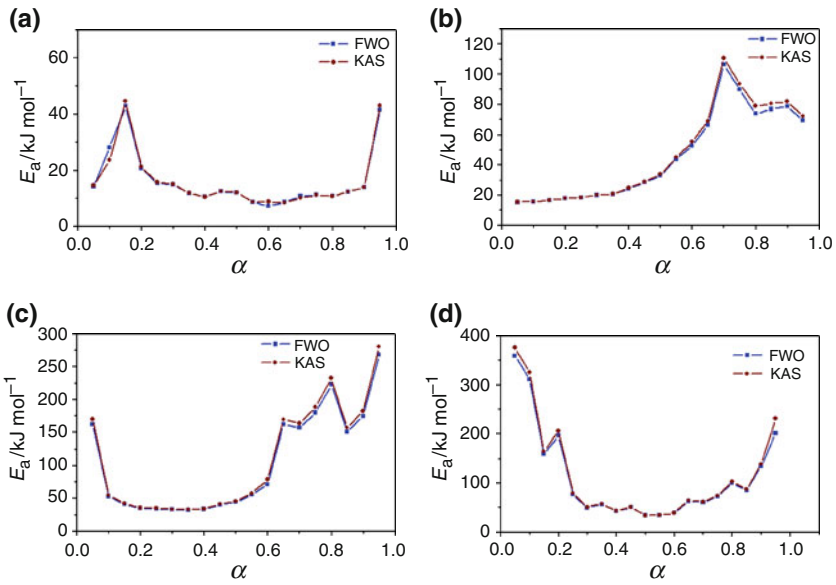

Fig. 5 The E^* versus α for the *cis*-[Ru(L_1)(L_2)(NCS)$_2$] complex based on model-free KAS and FWO methods: **a** the first decomposition stage, **b** the second decomposition stage, **c** the third decomposition stage, and **d** the fourth decomposition stage

Table 3 The activation energy, E^* values which calculated composite methods

Compound	Stage	Model	Composite model I			Composite model II		
			R^2	s.d.	E^*/kJ mol^{-1}	R^2	s.d.	E^*/kJ mol^{-1}
Ruthenium complex[a]	I	A2	0.980	3.35	33.26	0.975	2.49	29.43
	II	A3	0.965	2.24	60.92	0.980	3.51	56.03
	III	D1	0.962	3.43	125.08	0.970	2.79	116.61
	IV	D2	0.953	1.76	123.14	0.963	0.09	127.98

[a] *Cis*-[Ru(L_1) (L_2)(NCS)$_2$] complex

Table 4 The thermodynamic parameters for all decomposition stages

Compound	Stage	Method	Model	E^*/kJ mol^{-1}	LnA/kJ mol^{-1}	ΔH^*/kJ mol^{-1}	ΔS^*/J mol^{-1}	ΔG^*/kJ mol^{-1}
Ruthenium complex[a]	I	C.M I	A2	33.26	10.13	30.51	−156.14	84.94
		C.M II	A2	29.43	8.08	26.68	−173.18	86.75
	II	C.M I	A3	60.92	9.59	56.85	−169.27	143.86
		C.M II	A3	56.03	7.91	51.96	−183.24	110.03
	III	C.M I	D1	125.08	10.9	118.67	−161.45	240.03
		C.M II	D1	116.61	8.12	110.20	−184.57	248.02
	IV	C.M I	D2	123.14	10.32	115.42	−168.52	279.70
		C.M II	D2	117.98	8.06	110.26	−187.31	291.99

[a] *Cis*-[Ru(L_1) (L_2)(NCS)$_2$] complex

have E^* increase as α increases [33]. The average E^* values are 49.82, 48.38 kJ mol^{-1}, for KAS and FWO methods, respectively.

In stage III, the E^* values calculated by using KAS and FWO methods are quite similar, too. The E^* values decrease with increasing α up to $\alpha = 0.1$, and then remain relatively constant in the α-values between 0.1 and 0.5. Finally, the E^* values sharply increase in the $0.55 \leq \alpha \leq 0.95$ range (Fig. 5c). Therefore, it is concluded that the decomposition occurs multi-step except in the range of 0.1–0.5 where decomposition occurs only in one step. The average E^* values are 113.23, 108.82 kJ mol^{-1} for KAS and FWO methods, respectively.

In stage IV, the E^* values calculated by using KAS and FWO methods are quite similar, too. The E^* values decrease very fast up to $\alpha = 0.25$, and beyond this value it approximately remains stable up to 0.85. Finally, the E^* values increase up to $\alpha = 0.95$ and then decrease (Fig. 5d). Therefore, it is concluded that the decomposition occurs in only one step in 0.25–0.85 range. The average E^* values are 117.01, 112.09 kJ mol^{-1} for KAS and FWO methods, respectively.

The E^* and A have also been obtained using re-arranged KAS and FWO equations. The reaction models have been investigated by using thirteen kinetic model equations and the most suitable models have been selected. The E^* values, standard deviations, s.d. and regression analysis, r^2 values which calculated with composite methods are given in Table 3. The best model equations have been determined as A2, A3, D1, and D2. These model equations correspond to nucleation and growth mechanism for A2 and A3 and diffusion mechanism for D1 and D2 [34, 37]. The other thermodynamic parameters which have been calculated from the best model equations are presented in Table 4.

Conclusions

The final product has been identified as Ru and RuS_2 by XRD analysis. The pyrolytic decomposition mechanism of the *cis*-[Ru(L_1)(L_2)(NCS)$_2$] complex has been proposed depending on the thermogravimetric and mass results. The average E^* values for four decomposition stages are 19.98, 49.1, 11.03, and 114.55 kJ mol^{-1} as calculated using KAS and FWO methods. A comparison of the α dependent E^* of the *cis*-[Ru(L_1)(L_2)(NCS)$_2$] complex shows that the E^* values change α differently as α increases for all decomposition stages. Therefore, it is concluded that the decompositions contain multi-step process. The thirteen kinetic model equations have been treated for selecting the best model fitting equations. The best model equations have been obtained as A2, A3, D1, and D2. The optimized average values of E^* are 31.35, 58.48, 120.85, and 120.56 kJ mol^{-1} and the average values of Arrhenius factor, A, are 2.21, 2.61, 2.52, and 2.21 kJ mol^{-1} as calculated by using the best model equation for four decomposition stages, respectively. Also, the ΔH^*, ΔS^* , and ΔG^* have been obtained using these values.

References

1. Nazeeruddin MK, Humphry-Baker R, Liska P, Grätzel M. Investigation of sensitizer adsorption and the influence of protons on current and voltage of a dye-sensitized nanocrystalline TiO_2 solar cell. J Phys Chem B. 2003;107:8981–7.
2. Gratezel M. Conversion of sunlight to electric power by nanocrystalline dye-sensitized solar cells. J Photochem Photobiol A. 2004;164:3–14.
3. Ocakoglu K, Zafer C, Cetinkaya B, Icli S. Synthesis, characterization, electrochemical and spectroscopic studies of two new heteroleptic Ru(II) polypyridyl complexes. Dyes Pigment. 2007; 75:385–94.
4. Ocakoglu K, Yildirim Y, Lambrecht FY, Ocal J, Icli S. Biological investigation of 131I-labeled new water soluble Ru(II) polypyridyl complex. Appl Radiat Isot. 2008;66:115–21.
5. Ocakoglu K, Yakuphanoglu F, Durrant JR, Icli S. The charge transport and transient absorption properties of a dye-sensitized solar cell. Sol Energy Mater Sol C. 2008;92:1047–53.
6. Xie PH, Hou YJ, Zhang BW, Cao Y, Wu F, Tian WJ, Shen JC. Spectroscopic and electrochemical properties of ruthenium(II) polypyridyl complexes. J Chem Soc Dalton Trans. 1999;23: 4217–21.
7. Nazeeruddin MK, Zakeeruddin SM, Humphry-Baker R, Kaden TA, Gratezel M. Determination of pKa values of 4-phosphonato-2,20:60,200-terpyridine and its ruthenium(II)-based photosensitizer by NMR, potentiometric, and spectrophotometric methods. Inorg Chem. 2000;39:4542–7.
8. Rice CR, Ward MD, Nazeeruddin MK, Gratezel M. Catechol as an efficient anchoring group for attachment of ruthenium-polypyridine photosensitizers to solar cells based on nanocrystalline TiO_2 films. New J Chem. 2000;24:651–2.
9. Sahin C, Tozlu C, Ocakoglu K, Zafer C, Varlikli C, Icli S. Synthesis of an amphiphilic ruthenium complex with swallow-tail bipyridyl ligand and its application in nc-DSC. Inorg Chim Acta. 2008;361:671–6.
10. Amirnasr M, Nazeeruddin MK, Grätzel M. Thermal stability of *cis*-dithiocyanato(2,20-bipyridyl4,40dicarboxylate)ruthenium(II) photosensitizer in the free form and on nanocrystalline TiO_2 films. Thermochim Acta. 2000;348:105–14.
11. Rau S, Walther D, Vos JG. Inspired by nature: light driven organometallic catalysis by heterooligonuclear Ru(II) complexes. Dalton Trans. 2007;9:915–9.
12. Takeda H, Koike K, Inoue H, Ishitani O. Development of an efficient photocatalytic system for CO_2 reduction using rhenium(I) complexes based on mechanistic studies. J Am Chem Soc. 2008;130:2023–31.
13. Hayashi Y, Kita S, Brunschwig BS, Fujita E. Involvement of a binuclear species with the Re–C(O)O–Re moiety in CO_2 reduction catalyzed by tricarbonyl rhenium(I) complexes with diimine ligands: strikingly slow formation of the Re–Re and Re–C(O)O–Re species from Re(dmb)(CO)3S (dmb = 4,4′-dimethyl-2,2′-bipyridine, S = Solvent. J Am Chem Soc. 2003;125:11976–87.
14. Ocakoglu K, Emen FM. Thermal analysis of *cis*-(dithiocyanato)(1,10-phenanthroline-5,6-dione)(4,40-dicarboxy-2,20-bipyridyl)

ruthenium(II)photosensitizer. J Therm Anal Calorim. 2011;104 (3):1017–22.
15. Cilgi GK, Cetisli H. Thermal decomposition kinetics of aluminum sulfate hydrate. J Therm Anal Calorim. 2009;98:855–61.
16. Kücük F, Yildiz K. The decomposition kinetics of mechanically activated alunite ore in air atmosphere by thermogravimetry. Thermochim Acta. 2006;448:107–10.
17. Ozawa T. A new method of analyzing thermogravimetric data. Bull Chem Soc Jpn. 1965;38:1881–6.
18. Flynn JH, Wall LA. General treatment of the thermogravimetry of polymers. J Res Nat Bur Stand. 1966;70A:487–523.
19. Kissinger HE. Reaction of peak temperature with heating rate in different thermal analysis. J Res Nat Bur Stand. 1956;57:217–21.
20. Kissinger HE. Reaction kinetics in differential thermal analysis. Anal Chem. 1957;29:1702–6.
21. Akahira T, Sunose T. Joint convention of four electrical institutes. Res Rep Chiba Inst Technol. 1971;16:22–31.
22. Simon P. Isoconversional methods; fundamentals, meaning and application. J Therm Anal Calorim. 2004;76:123–32.
23. Koç S, Toplan N, Yildiz K, Toplan H. Effects of mechanical activation on the non-isothermal kinetics of mullite formation from kaolinite. J Therm Anal Calorim. 2011;103:791–6.
24. Wu W, Wu X, Lai S, Liao S. Non-isothermal kinetics of thermal decomposition of $NH_4ZrH(PO_4)_2{\cdot}H_2O$. J Therm Anal Calorim. 2011;104:685–91.
25. Sovizi MR, Anbaz K. Kinetic investigation on thermal decomposition of organophosphorous compounds. J Therm Anal Calorim. 2010;99:593–8.
26. Stefano V, Romolo DR, Carla F. Kinetic study of decomposition for Co(II)- and Ni(II)-1,10-phenanthroline complexes intercalated in c-zirconium phosphate. J Therm Anal Calorim. 2009;97: 805–10.
27. Muraleedharan K, Kanan M, Ganga DT. Thermal decomposition kinetics of potassium iodate. J Therm Anal Calorim. 2011;103: 943–55.
28. Uemura K, Kitagawa S, Saito K, Fukui K, Matsumoto K. Thermodynamic aspect of reversible structural conversion induced by guest adsorption/desorption based on infinite $Co(NCS)_2Py_4$ (Py = pyridine) system. J Therm Anal Calorim. 2005;81:529–32.
29. Alvarez V, Rodriguez E, Vazquez A. Thermal degradation and decomposition of jute/vinylester composites. J Therm Anal Calorim. 2006;85:383–9.
30. Guinesi LS, Ribeiro CA, Crespi MS, Santos AF, Capela MV. Titanium(IV)-EDTA complex. J Therm Anal Calorim. 2006;85: 301–7.
31. Jun Z, Shuangjun C, Jing J, Xuming S, Xiaolin W, Zhongzi X. Non-isothermal melt crystallization kinetics for ethylene–acrylic acid copolymer in diluents via thermally induced phase separation. J Therm Anal Calorim. 2010;101:243–54.
32. Banjong B. Kinetic and thermodynamic studies of $MgHPO_4{\cdot}3H_2O$ by non-isothermal decomposition data. J Therm Anal Calorim. 2009;98:863–71.
33. Huang JW, Chang CC, Kang CC, Yeh MY. Crystallization kinetics and nucleation parameters of Nylon6 and poly(ethylene-co-glycidyl methacrylate) blend. Thermochim Acta. 2008;468:66–74.
34. Vyazovkin S, Burnham AK, Criado JM, Maqueda LAP, Popescu C, Sbirrazzuoli N. ICTAC Kinetics Committee recommendations for performing kinetic computations on thermal analysis data. Thermochim Acta. 2011;520:1–19.
35. Gabal MA. Non-isothermal studies for the decomposition course of CdC_2O_4–ZnC_2O_4 mixture in air. Thermochim Acta. 2004;412: 55–62.
36. Budrugeac P, Segal E. On the use of Diefallah's composite integralmethod for the non-isothermal kinetic analysis of heterogenous solid-gas reactions. J Therm Anal Calorim. 2005;82: 677–80.
37. Brown ME, Maciejewski M, Vyazovkin S, Nomen R, Sempere J, Burnham A, Opfermann J, Strey R, Anderson HL, Kemmler A, Keuleers R, Janssens J, Desseyn HO, Li CR, Tang TB, Roduit B, Malek J, Mitsuhashi T. Computational aspects of kinetic analysis part A: the ICTAC kinetics project-data, methods and results. Thermochim Acta. 2000;355:125–43.
38. Vyazovkin S, Wight CA. Kinetics in solids. Annu Rev Phys Chem. 1997;48:125–49.